

SIMULATION OF PILOT CONTROL ACTIVITY DURING HELICOPTER SHIPBOARD OPERATION

Dooyong Lee*, Joseph F. Horn†, Nilay Sezer-Uzol‡, Lyle N. Long§

Department of Aerospace Engineering
The Pennsylvania State University
University Park, PA 16802

Abstract

A simulation of the helicopter/ship dynamic interface has been developed and applied to simulate a UH-60A operating from an LHA class ship. Time accurate CFD solutions of the LHA airwake are interfaced with a flight dynamics simulation based on the GENHEL model. The flight dynamics model was updated to include improved inflow modeling and gust penetration effects of the ship airwake. An optimal control model of a human pilot was used to simulate pilot control activity for a specified approach trajectory. The pilot model was designed so that the tracking performance could be tuned based on a desired crossover frequency in each control axis. The model was used to predict pilot workload for shipboard approaches in two different wind-over-deck conditions. Although further validation is needed, preliminary results show that the simulation results in similar workload trends as recent flight test studies.

Introduction

Helicopter shipboard launch and recovery operations continue to be a topic of interest for both civil and military operators. Ship-based helicopters regularly operate under hazardous flight conditions. Highly turbulent airwakes from the ship's superstructure, low visibility, and moving flight decks make helicopter shipboard operations one of the most challenging, training intensive and dangerous of all helicopter flight operations.

To ensure the compatibility of a particular helicopter and ship under various operating conditions, extensive dynamic interface flight-testing must be performed. This approach is both costly and limited by the availability of fleet assets and weather conditions. For example, the wind-over-the-deck (WOD) envelope defines the allowable wind conditions in terms of speed and azimuth for a given helicopter ship combination.

The envelope is established by performing a series flight tests for all possible combinations of wind speed and azimuth (typically in 5 knot, 15 deg increments) and taking subjective pilot ratings. The WOD envelopes are often overly restrictive, because certain wind conditions never present themselves during tests.

Better simulation tools for analyzing shipboard operations might be used for a variety of purposes. Simulation testing can be used for pilot training and to reduce flight test time and cost for establishing safe WOD envelopes. Ultimately piloted simulation testing might be used in acceptance testing of future rotorcraft and future ships.¹ In addition to the piloted simulation applications, the development of a non-real-time simulation tool for use in engineering and design would also be valuable. Such a simulation tool could be used to find optimal approach paths for safe landings, to design and test new flight control systems, and to identify possible trouble spots for future ship and helicopter combinations early in the design phase. Three key elements of this simulation tool include: CFD representations of the time varying ship airwake, a high fidelity flight dynamics model of the helicopter, and a feedback control model of the human pilot.

Understanding and modeling the airwake from complex ship geometries presents a number of technical challenges. Some of the key flow features of the airwake are: unsteadiness, large regions of separated flow, vorticity, and low Mach number. Previous researchers have performed numerous experimental and computational studies of airwakes for different classes of ships. The U.S. Navy has done some experimental investigations using both full-scale tests and scale-model tests in wind tunnels.² Unfortunately it is both difficult and costly to obtain high quality and complete sets of airwake data for all of the different WOD conditions on any given ship. Computational simulations of ship airwakes provide an attractive alternative and have been performed using a number of different numerical approaches by Tai,³ Tattersall *et al.*,⁴ Liu and Long,⁵ Guillot and Walker,⁶ and Reddy *et al.*⁷ Recently Sharma and Long⁸ have simulated inviscid, steady and time-accurate flow over an LPD-17 ship using a modified parallel flow solver PUMA. They found good agreement between the steady-state solution

* Graduate Research Assistant, dylee@psu.edu

† Assistant Professor, joehorn@psu.edu

‡ Graduate Research Assistant, nxs216@psu.edu

§ Professor, lnl@psu.edu

Copyright © 2003 The American Institute of Aeronautics and Astronautics Inc. All rights Reserved

and frequency spectrum of from wind tunnel experiments. Polsky and Bruner^{9,10} have investigated LHA ship airwakes using the parallel unstructured flow solver COBALT with different numerical methods such as laminar Navier-Stokes and MILES as well as $k-\omega$ and SST turbulence modeling. It was shown that steady-state CFD calculations were unable to predict the time average of the turbulent flow field, and observed that turbulence modeling added too much dissipation to the calculation since the flux-splitting numerical schemes are very dissipative. Bogstad *et al*¹¹ have solved for inviscid flow around six different ships of the Royal Navy to obtain an airwake database for a helicopter flight simulator (Merlin). Camelli *et al*¹² have performed an LES simulation of airwake and stack gas temperature field around the LPD-17 class ship using a Smagorinsky turbulence model.

A number of recent research programs have also focused on the simulation of helicopter flight dynamics during shipboard operations, with the goal of assessing handling qualities and pilot workload.¹³⁻¹⁶ The Joint Shipboard Helicopter Integration Process (JSHIP) has been applied to increase the interoperability of joint shipboard helicopter operations for helicopters that are not specifically designed to go aboard Navy ships.^{13,14} As a part of JSHIP, the Dynamic Interface Modeling and Simulation System (DIMSS) was established to define and evaluate a process for developing WOD flight envelopes. Using DIMSS, the fidelity standards for the shipboard launch and recovery task has been discussed for combination of an LHA class ship and a UH-60.¹⁴

Over the last several decades, the extensive effort in developing feedback control theory has also proven to be quite useful in quantifying control-related human behavior.¹⁷ The so-called “crossover model” employs classical control methods to model human feedback control of SISO systems. The method is based on the expected crossover frequency of the open loop transfer function of the human and controlled process. In fact, Bradley and Turner applied the crossover model, coupled with inversion control methods, specifically to model pilot workload for helicopter shipboard operations.¹⁹ The main drawback of the crossover model is that the helicopter piloting task is inherently MIMO. Although extensions of the classical crossover model can be applied to MIMO systems, the use of modern MIMO control theory can be more convenient, particularly since the design algorithms are readily automated using modern software such as MATLAB. The optimal control model (OCM) of the human pilot is applied for control of MIMO systems by solving the Linear Quadratic Gaussian problem. It has been shown that this approach had direct correlations with the

classical crossover model, but is more readily applied to MIMO systems, and that the weighting coefficients can be derived based on desired crossover frequency.¹⁸

In this study, a dynamic interface simulation of the UH-60A helicopter operating off an LHA is developed. This represents the same aircraft ship combination used in the JSHIP program. The objective of this study is to understand the impact of a time-varying ship airwake on the pilot control activity for an approach operation, and to develop a human pilot model for analyzing the pilot workload. Previous studies have shown that the time varying nature of the ship airwake has significant effect on control activity for approach operations.^{20, 21} The Parallel Unstructured Maritime Aerodynamics CFD solver (PUMA2) is used to calculate the flow over the LHA. Both the temporal and spatial variations of the unsteady wake are accounted for in the flight dynamics simulation. An optimal control model of a human pilot is used to simulate the control inputs required to perform a specified approach, and the qualitative effects of WOD conditions on pilot control activity are explored.

Dynamic Interface Simulation Model

Ship Airwake Model – CFD Flow Solver

The helicopter simulation is integrated with time-accurate CFD solutions of the airwake of an LHA class ship. The Parallel Unstructured Maritime Aerodynamics CFD solver (PUMA2) is used to calculate the flow. It uses a finite volume formulation of the Euler/Navier-Stokes equations for 3-D, internal and external, non-reacting, compressible, steady/unsteady solutions for complex geometries. PUMA2 can be run so as to preserve time accuracy or as a pseudo-unsteady formulation to enhance convergence to steady state. It is written in ANSI C using the MPI library for message passing so it can be run on parallel computers and clusters. It is also compatible with C++ compilers and coupled with the computational steering system POSSE.²² It uses dynamic memory allocation, thus the problem size is limited only by the amount of memory available on the machine. Large eddy simulations can also be performed with PUMA2.^{22,23}

Helicopter Flight Dynamic Model

The flight dynamics model is based on the GENHEL model of the UH-60A.²⁴ To facilitate model improvement and control law development, a MATLAB/SIMULINK based version was developed.²⁰ The simulation model is divided into sub-modules that represent the aerodynamics and dynamics of various helicopter components (e.g. main rotor, fuselage,

empennage, and tail rotor). The simulation uses a total force, large angle representation of the six rigid body degrees of freedom of the fuselage. The main rotor module includes rigid rotor blade flapping, lagging, and rotational degrees of freedom as well as an air mass degree of freedom. In this study, the model was updated to include a high order Peters-He dynamic inflow model.²⁵ In this paper, a 15 state inflow model is used.

The primary flight control system of the UH-60A is a mechanical system with a mixing unit that helps mitigate cross-coupling effects. The aircraft also uses a full authority automatic stabilizer. The Automatic Flight Control System (AFCS) includes a limited authority Stability Augmentation System (SAS) in the pitch, roll, and yaw axes. The Flight Path Stabilization (FPS) is a full-authority, rate limited autopilot that operates by back driving the pilot control sticks. In this study, the aircraft is modeled with the SAS engaged and the FPS disengaged. An analytical definition of the control system is given in Ref. 24.

Gust Penetration Model

The gust penetration model is used to model the effects of a three-dimensional ship airwake on the helicopter flight dynamics. There is a fundamental assumption that the velocity field of the airwake affects the aerodynamic forces on the aircraft, but the aircraft does not affect the ship airwake. The velocity field is determined at all of the distributed components on the helicopter. Thus the location of all of the components must be computed at each point in time relative to the ship. To account for local velocities at the rotor blade elements, fuselage, empennage and tail rotor, a 3-dimensional interpolation algorithm is applied. The ship airwake velocity field provided by the CFD database is defined with respect to a ship-fixed coordinate system. Thus, the velocity field must be transformed to inertial axes, and then to the specific axis systems used for each of the helicopter component models. For the fuselage,

empennage and tail rotor, the following coordinate transformation is required.

$$\vec{V}_{body} = \mathbf{T}_{i2b} \mathbf{T}_{s2i} \vec{V}_{ship} \quad (1)$$

where \vec{V}_{ship} is the ship wake velocity in ship coordinate system, \vec{V}_{body} is the ship wake velocity in the helicopter body coordinate system, \mathbf{T}_{s2i} is the coordinate transformation matrix from ship coordinate system to inertial coordinate system and \mathbf{T}_{i2b} is the coordinate transformation matrix from inertial to helicopter body coordinate system.

For each main rotor blade element, the following coordinate transformation is required.

$$\vec{V}_{rotor} = \mathbf{T}_{h2b} \mathbf{T}_{b2h} \mathbf{T}_{i2b} \mathbf{T}_{s2i} \vec{V}_{ship} \quad (2)$$

where \vec{V}_{rotor} is the ship wake velocity in blade coordinate system, \mathbf{T}_{b2h} is the coordinate transformation matrix from helicopter body to hub coordinate system, \mathbf{T}_{h2b} is the coordinate transformation matrix from hub to each blade coordinate system. These transformations must account for the orientation of the helicopter, the hub, and all of the rotor degrees of freedom.

The time-varying components of the airwake are stored at every 0.1 seconds for a total of 40 seconds of time history. Linear interpolation is used to calculate the gust field at every simulation time step (0.01 seconds). Since the maneuvers generally last longer than 40 seconds, the whole time accurate flow solutions must be repeated. To prevent the sudden jump at every 40 seconds period, the solutions are overlapped with sinusoidal filter for first and last 5 seconds.

Optimal Control Model of a Human Pilot

Figure 1 represents a simplified optimal control model of a human pilot. In this study, the human pilot's

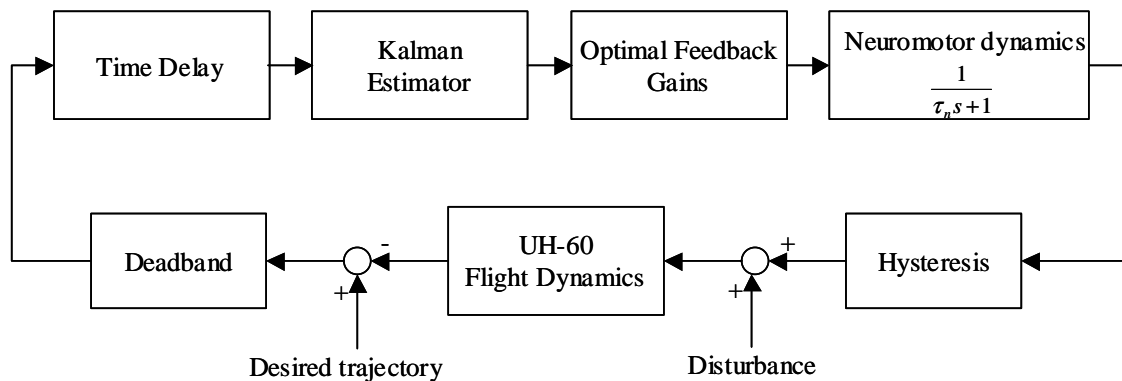


Figure 1 Optimal control model of the human pilot

basic task is to control the aircraft to follow a specified approach trajectory. To design the human control model, the aircraft is represented with linearized equations of motion in state variable form:

$$\begin{aligned}\dot{\mathbf{x}}(t) &= \mathbf{A}\mathbf{x}(t) + \mathbf{B}\mathbf{u}(t) + \mathbf{w}(t) \\ \mathbf{y}(t) &= \mathbf{C}\mathbf{x}(t) + \mathbf{v}(t)\end{aligned}\quad (3)$$

where $\mathbf{x}(t)$ is the state vector, $\mathbf{u}(t)$ is the pilot's control input vector, $\mathbf{w}(t)$ is a vector of external disturbances, $\mathbf{y}(t)$ is vector of measurements (parameters perceived by the pilot), and $\mathbf{v}(t)$ represents observation noise. The human pilot model in Figure 1 is represented as an optimal linear regulator in combination with an optimal state estimator (Kalman estimator). Both the estimator and feedback gain matrix are determined by solving the Linear Quadratic Gaussian control problem. Assuming the linear dynamics of equation 3 and the disturbance are white noise signals, the objective is to find a dynamic compensator that minimizes the quadratic performance index given by:

$$J = E \left\{ \lim_{T \rightarrow \infty} \frac{1}{T} \int_0^T [\mathbf{x}^T(t) \mathbf{Q} \mathbf{x}(t) + \dot{\mathbf{u}}(t) \mathbf{R} \dot{\mathbf{u}}(t)] dt \right\} \quad (4)$$

where \mathbf{Q} and \mathbf{R} are the state and control weighting matrices. The estimator and feedback gains are readily solved from a pair of matrix Riccati equations. Note that when modeling human operators it is customary to use control rates instead of the control position in the performance index. A simple augmentation of the plant dynamics model is used to achieve this.¹⁷ Details of the complete optimal control model of the human operator are discussed in Ref. 17 and 18.

A numerical linearization of the simulation model is used to obtain a 24 state model, which includes 9 rigid body states and 15 states associated with rotor dynamics and inflow. For this study, the model was linearized about a hover equilibrium in a 30 knot wind (which represents the terminal phase of the approach maneuver). Assuming quasi-static rotor and inflow dynamics, the linear model is reduced to a 9 state / 6 DOF model of the rigid body motion. The linear model is decoupled into a 3 state longitudinal model, a 5 state lateral-directional model, and a 1 state vertical motion model. Finally, the linear models must be augmented to include shaping filters for the gust disturbances and a dynamic model of the SAS for each axis. Integrators are added so that position and integrated position can be included in the performance index. A schematic of the augmented flight dynamics model used for longitudinal control is shown below. A similar model was used for

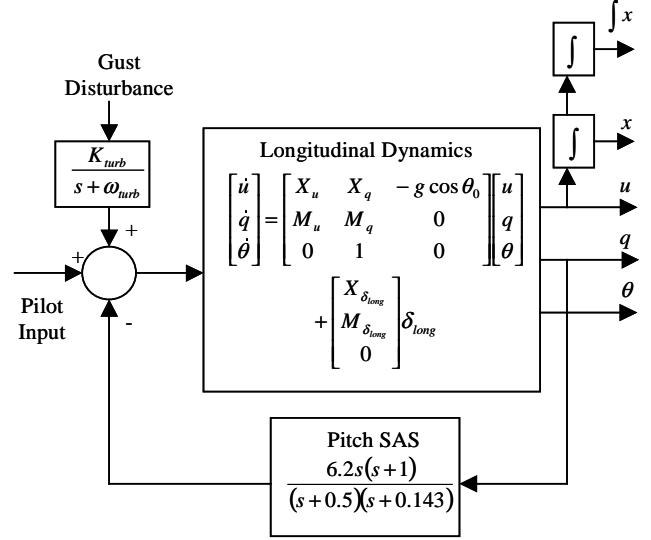


Figure 2 Augmented plant model in longitudinal axis

lateral-directional control, which includes pilot inputs in both the lateral and directional axes.

A key task in developing an appropriate optimal control model of the human pilot is the selection of the appropriate weighting matrices, \mathbf{Q} and \mathbf{R} . The effect of the parameter weighting parameters is not as clear as in the case of the crossover model of the human operator, because the optimal control model parameters are essentially inputs to an optimization scheme that involves the solution of sets of nonlinear algebraic equations.¹⁸ However, reference 18 outlines an approximate method for selecting these parameters to achieve a desired crossover frequency for each control axis.

Typically, both the \mathbf{Q} and \mathbf{R} matrices are assumed to be diagonal. The weighting parameters in the \mathbf{Q} matrix are selected such that each state variable is scaled by its maximum expected deviation.¹⁸ This leaves the task of selecting the control weighting parameters in \mathbf{R} . In this study, the objective was to develop a pilot model that could be easily tuned to adjust the tracking tolerance in each control axis, where a high crossover frequency corresponds to “tight” tracking and a low crossover frequency corresponds to “relaxed” tracking.

Consider the longitudinal axis where the transfer function from longitudinal control input to pitch attitude can be expressed as:

$$\frac{\theta}{\delta_{long}}(s) = \frac{K(s^m + a_{m-1}s^{m-1} + \dots + a_1s + a_0)}{(s^n + b_{n-1}s^{n-1} + \dots + b_1s + b_0)} \quad (5)$$

An approximate but very useful relationship exists between the weighting coefficients, the controlled-

element dynamics, and the closed-loop system bandwidth:^{17, 18}

$$\omega_{BW} \approx \left[K(q_\theta / r_{\delta_{long}})^{1/2} \right]^{(n-m+1)} \quad (6)$$

where q_θ is the weighting parameter for pitch attitude, r_δ is the longitudinal control weighting, and ω_{BW} is closed-loop bandwidth (frequency where the amplitude of the closed-loop transfer function is 6dB below its zero-frequency value). The following is an approximate relation between the open-loop crossover frequency and the closed-loop bandwidth:

$$\omega_c \approx 0.56\omega_{BW} \quad (7)$$

Thus, given a desired crossover frequency in each control axis, equations 5, 6, and 7 provide a method of determining appropriate control weighting parameters in **R**.

Figure 1 also includes blocks labeled neuromotor dynamics and time delay. These terms can be used to account for the physiological limitations on the ability of human pilots to make corrective actions. In this study a time constant $\tau_n = 0.1$ was used, and the time delay was set to 0.1 sec. These are typical values used in modeling human performance.¹⁷

Control records from human helicopter pilots have shown that there is a stepped appearance in the collective control input.¹⁹ Pilots tend to make discrete rather than continuous adjustments to the collective lever. This effect can be modeled using nonlinear elements in the pilot model. A hysteresis is attached to the control leading to the helicopter and deadband is placed across the error prior to its processing by the control model. These elements represent an error threshold for which the pilot recognize a departure from the desired trajectory. It should be noted that these nonlinear elements are incorporated only with collective control.

Shipboard Approach Trajectory

In this study, a typical shipboard approach trajectory was simulated. Kinematic profiles of this shipboard task are given in Ref. 16. The profile is modified slightly to be consistent with approach maneuvers used in the JSHIP study. The kinematic profile is determined using an Earth fixed coordinate frame with the origin at the sea surface directly under the initial position of the helicopter. The X-axis is along with the North direction, Z-axis is downward, and Y-axis is along with the East direction. The target spot is spot 8 of the LHA class ship (see Figure 3).

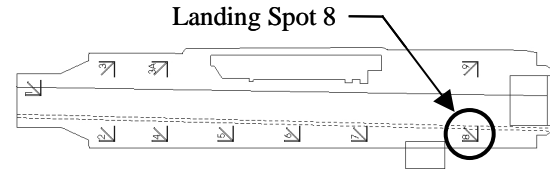


Figure 3 Top view of LHA class ship

Typical shipboard approach procedures include all actions that bring the rotorcraft from a point far away from the ship down to a point much closer to the recovery spot.^{13,16} The development of the kinematics profile for a shipboard approach is presented in Refs. 13,19. The entire shipboard approach task can be divided into three phases:

1. Phase I: From steady level flight, the helicopter transitions to a desired descent rate and horizontal deceleration.
2. Phase II: The helicopter maintains a constant descent rate and horizontal deceleration.
3. Phase III: The descent rate and horizontal deceleration are reduced to zero, ending in stationkeeping over a landing spot.

The key parameters for defining the approach profile are the helicopter initial level flight speed, initial altitude, initial distance from the ship, and desired final altitude for stationkeeping. The general profile parameters of the shipboard approach are shown in Table 1.

Table 1 Initial profile parameters

Initial altitude	300 ft
Final altitude	80 ft
Initial speed	60 knot
Final speed	0 knot

In his study, the helicopter approaches the ship from the port side at a 45° angle, and then performs a 45° left turn to align itself with the longitudinal axis of the ship after it crosses over the deck. This is similar to the trajectory used in the JSHIP study. For simplicity, the ship is assumed to be stationary in a 30 knot steady wind. Both a head wind and a wind from 30° starboard of the bow are considered.

Simulation Results

CFD Simulation of Ship Airwake

The simulation model is interfaced with steady-state and time-accurate inviscid CFD predictions for an LHA ship airwake. Figure 4 shows the 3-D unstructured grid for the full-scale LHA geometry, which is generated using the GRIDGEN software. The rectangular computational grid has 854,072 cells. The flow case represents both 0 and 30 degrees yaw angles and 30 knot of relative wind speed. These are the same cases simulated by Polsky and Bruner.⁹ A 4-stage Runge-

Kutta explicit time integration algorithm with Roe's flux difference scheme is used with CFL numbers of 2.5 and 0.8 for the steady and unsteady computations, respectively. A zero-normal-velocity boundary condition is applied on the ship surface and water surface (bottom surface of the domain) and a Riemann boundary condition is applied at all other faces of the domain. The pseudo steady-state computations are performed using local time-stepping and initialized with freestream values. The time accurate computations are started from the pseudo steady-state solution, and the simulation time step (480 μ sec) is determined by the smallest cell size in the volume grid. The computations are performed on a parallel PC cluster Lion-11 consisting of 256 2.4 Ghz P4 processors with 4 GB ECC RAM and Quadrics high-speed interconnect. It takes nearly 2080 iterations to simulate 1 second of real flow (~1.8 hours on 12 processors) with the current grid.

The time-accurate CFD solutions result in large quantities of time history data that need to be mapped into the DI simulation gust penetration model. Thus, for a given launch or recovery operation, the velocity data can be mapped into a rectangular grid (to allow easy table look up) and stored for only that part of the ship where the aircraft is expected to fly. Figure 5 shows the rectangular volumetric domain of CFD data over the rear deck of LHA for DI simulations. The DI mesh has (81x30x23) grid points with 5ft equal intervals. The DI mesh is selected to have the flow data over landing spots 7 and 8. A total of 50 seconds of time-accurate flow solution is obtained. Only the last 40 seconds of the time history data is stored for every 0.1 seconds to be used for the DI simulations. Each flow solution file is 41 Mbytes in size, whereas the DI velocity data is only 5.2 Mbytes.

Iso-surfaces of vorticity magnitude for both 0 and 30 degrees WOD cases are shown in Figure 6. Similar features can be observed as in Ref. 9 such as bow separation, deck-edge vortices, complex island wake for both cases, and burbles in the flow field between the bow separation and the island for the zero-yaw case. For the 30 degree WOD case, more complex island wake can be observed especially over the landing spots 7 and 8. Figure 7 (a) shows time history of velocity magnitude at a selected point in the DI mesh over landing spot 8 for 0 and 30 degrees yaw cases. The velocity data at that point, which is located at (-90ft, -35ft, 17ft), is extracted from the 40 seconds of real flow solutions with 0.1 seconds of intervals. The power spectrum of the velocity magnitude, non-dimensionalized by the square of the freestream velocity, versus Strouhal number (calculated using the ship length and freestream velocity) is plotted in Figure 7 (b) for 0 and 30 degrees yaw cases. Power spectra of 30 degree yaw case generally has more amplitude than

the 0 degree yaw case probably due to larger vortical structures present in the wake.

Dynamic Interface Simulation Results

The dynamic interface flight dynamics model has been applied to simulate a UH-60A approach to an LHA class ship (using the approach trajectory described above). The simulation was performed for two different airwake conditions (30 knot winds at 0° WOD and 30° WOD).

The optimal control model of the pilot was designed for three different levels of tracking performance by varying the desired crossover frequency of the open-loop transfer function in the pitch, roll, and yaw axes. The three different cases are termed 'normal', 'relaxed', and 'tight' tracking. Table 2 summarizes the desired and actual crossover frequencies for each case and each control axis.

Table 2 Crossover frequencies (rad/sec)

	Longitudinal	Lateral	Yaw
	Desired	Desired	Desired
	Actual	Actual	Actual
Case 1 (normal)	1.0	1.5	1.5
	1.23	1.47	2.16
Case 2 (relaxed)	0.5	1.0	1.0
	0.64	0.98	1.58
Case 3 (tight)	1.25	1.75	1.80
	1.49	1.73	2.43

As shown in Table 2, the actual crossover frequencies are slightly different than the desired crossover frequencies specified in the OCM design, due to the approximate nature of equations 5-7. However, in this study it is not considered necessary to specify exact values, only to develop a 'tunable' human pilot model and observe the relative behavior for different levels of tracking precision. More exact representations of the human pilot can be implemented once more detailed validation data is available.

Figures 8-10 show the simulation results for the approach in the two different WOD conditions with the Case 1 (normal) pilot model. The conventions for pilot control positions are as follows; full left lateral cyclic, full forward longitudinal cyclic, full down collective pitch, and full left pedal correspond to 0%, full right lateral cyclic, full aft longitudinal cyclic, full up collective pitch, and full right pedal correspond to 100%.

Figure 9 shows the tracking error relative to the specified approach trajectory, and the results indicate that the tracking performance of the pilot model is reasonable for both cases. As expected, the attitude changes and control activity are fairly benign in the early part of the maneuver, when the helicopter is relatively far from the ship. Near the end of the maneuver, the helicopter begins to interact significantly with the time-varying airwake, as indicated by the fluctuations in attitude and increased control activity. The 30° WOD condition results in significantly larger oscillations and higher pilot control activity, particularly when hovering over the ship deck. This reflects the so-called a cliff edge effect¹³, where strong shear layers from the island are blown across the spot with winds from 30 degrees.

Figures 11 and 12 show the simulation results for different pilot models performing the approach maneuver in 30° WOD conditions. Figures 13 and 14 shows similar results for the aircraft hovering over spot 8 in 30° WOD condition. The results indicate that when using a lower crossover frequency, as in case 2 (relaxed), there are significantly larger errors in the tracking but less control activity. This would represent a situation where the pilot is under controlling, and allowing the airwake turbulence to move the aircraft about with relatively little compensation. On the other hand, when using a higher crossover frequency, as with the case 3 (tight), there is actually relatively little improvement in tracking performance, but significantly more control activity. This might be example of a pilot over controlling the aircraft, increasing workload with relatively little payoff in terms holding the desired trajectory.

Unfortunately, as of the publication of this paper, detailed validation data from the JSHIP flight test program was not available to the authors. However, some limited qualitative and quantitative comparisons can be made with the published data of Roscoe and Wilkinson.^{13, 14}

When establishing WOD envelopes, the U.S. Navy uses a subjective rating system called the Deck Interface Pilot Effort Scale (DIPES). The DIPES rating describes the pilot workload in relation to the level of performance achieved, where DIPES 1 indicates slight to moderate workload and DIPES 5 represents extreme workload. DIPES ratings of 1, 2, and 3 are considered acceptable, DIPES 4 and 5 are considered unacceptable and would eliminate a given condition from the WOD envelope for a given ship / helicopter combination. It is interesting to note that during JSHIP flight testing from landing spot 8, 30 knot relative winds at 0° yaw angle resulted in DIPES 1 or 2. While 30 knot relative winds at 30° yaw angle resulted a DIPES rating of 4.

Qualitatively, these subjective ratings are consistent with the results in this study.

In the work by Roscoe and Wilkinson they developed quantitative metrics that showed reasonable correlation with the subjective DIPES ratings.¹³ Of particular interest was the standard deviation of the control deflections as calculated over a running 3 second window, and the number of control reversals over a 3 second window. Together these two metrics provide measures of the amplitude and frequency of the control movements respectively. It was found that the DIMMS product metric, which is simply the product of these two metrics averaged over an entire maneuver, showed strong correlation with DIPES ratings for any given pilot. However, it was found that there was significant variation in the DIMMS product metric for different pilots.

The DIMSS product metric was evaluated for the pitch, roll, and yaw axes using the Case 3 pilot model (tight tracking) for both the 0° and 30° WOD conditions. Figure 15 shows sample control reversals and standard deviation metrics in the lateral axis versus time for the approach maneuver in 30° WOD. As done in the JSHIP study, only the last phase of the maneuver, where the helicopter crosses the ship deck, is considered. These results were converted to DIMSS product metrics in each axis. The results in reference 13 provide the average DIMSS product metric for all of the maneuver given DIPES ratings of 1, 2, and 4 (these were the only ratings given in the flight tests). The paper indicates that most of the 30 knot, 0° WOD landings for spot 8 were given DIPES 1, while the only DIPES 4 rating was for the 30 knot, 30° WOD case. Figures 16-17 compares the DIMSS product metrics in the lateral and longitudinal axes from the JSHIP flight test data to those from the simulation results in this paper (assuming the 0° WOD case is DIPES 1 and the 30° WOD case is DIPES 4). Although the simulation resulted in lower values of the DIMSS product metric, the trend between the 0° and 30° WOD cases is similar to that of the flight tests. The JSHIP study showed that the DIMSS product metric varied significantly from pilot to pilot, while showing a consistent trend with DIPES for each pilot. It could also be expected that further tuning of the OCM pilot could produce similar values as the human pilots from the JSHIP study.

Conclusions

A helicopter/ship dynamic interface simulation tool has been developed to model a UH-60A operating off an LHA class ship. To achieve a high fidelity simulation model, time-accurate ship airwake solutions of an LHA class ship are integrated with an established flight dynamics simulation model. These ship airwake

solutions are calculated using PUMA2. Both 0 degree and 30 degree WOD time-accurate inviscid ship airwake flow fields are calculated for the 3 dimensional full-scale LHA geometry. Approach and hovering operations were simulated from landing spot 8 on the LHA. (CFD results showed significant time-varying flow effects over this spot). An optimal control model of the human pilot was developed to perform the maneuvers with different levels of tracking performance. Results were compared for the 0° and 30° WOD conditions, and for three different levels of tracing performance. Pilot control activity was compared to JSHIP flight test data in terms of the DIMSS product metric. Based on these results the following conclusions can be made:

1. Time varying airwake effects seem to have a significant impact on pilot control activity. The 30° WOD condition showed a substantial increase in pilot workload. This is backed up by JHSIP flight test data.
2. The optimal control model of the human pilot proved to be an efficient method for simulating approach trajectories. The pilot model was easily tuned and seemed to produce reasonable predictions of trajectory tracking and pilot control activity.
3. Preliminary comparisons with quantitative workload metrics collected during the JSHIP program are encouraging. The OCM representation of the pilot seems to produce similar trends with respect to DIMSS workload metric. However, it is desirable to obtain more detailed validation data to prove the capability of the simulation tool developed in this study.

References

1. Mello, O.A.F., Prasad, J.V.R. and Sankar, L.N., Tseng, T., "Analysis of Helicopter/Ship Aerodynamic interactions," The American Helicopter Society Aeromechanics Specialists Conference, San Francisco, CA, January 19-21, 1994.
2. Zan, S.J., Syms, G.F., and Cheney, B.T., "Analysis of Patrol Frigate Air Wakes," Presented at the NATO RTO Symposium on Fluid Dynamics Problems of Vehicles Operating near or in the Air-Sea Interface, Amsterdam, The Netherlands, October 5-8, 1998.
3. Tai, T.C., "Simulation and Analysis of LHD Ship Airwake by Navier-Stokes Method," Presented at the NATO RTO Symposium on Fluid Dynamics Problems of Vehicles Operating near or in the Air-Sea Interface, Amsterdam, The Netherlands, October 1998.
4. Tattersall, P, Albone, C M, Soliman, M M, Allen, C B, "Prediction of Ship Air Wakes over Flight Decks using CFD," In AGARD Fluid Dynamics Symposium on Fluid dynamics of Vehicles Operating Near or In the Air-Sea Interface, Paper No.6, Amsterdam, October 1998.
5. Liu, J. and Long, L.N., "Higher Order Accurate Ship Airwake Predictions for the Helicopter-Ship Interface Problem," Presented at AHS 54th Annual Forum, Washington D.C., May 20-22, 1998.
6. Guillot, M.J., Walker, M.A., "Unsteady Analysis of the Air Wake over the LPD-17," AIAA Paper 2000-4125, AIAA Applied Aerodynamics Conference and Exhibit, 18th, Denver, CO, Aug. 14-17, 2000.
7. Reddy, K.R., Toffoletto, R., Jones, K.R.W., "Numerical simulation of ship airwake," *Computers and Fluids*, Vol29, p451-465, 2000.
8. Sharma, A. and Long, L.N., "Airwake simulations on an LPD 17 ship," AIAA Paper 2001-2589, AIAA Computational Fluid Dynamics Conference, 15th, Anaheim, CA, June 11-14, 2001.
9. Polsky, S. A., Bruner, C. W. S., "Time-Accurate Computational Simulations of an LHA Ship Airwake," *AIAA Paper 2000-4126*, 18th AIAA Applied Aerodynamics Conference, Denver, CO, Aug. 14-17, 2000.
10. Polsky, S.A., "A Computational Study of Unsteady Ship Airwake," AIAA Paper 2002-1022, 40th AIAA Aerospace Sciences Meeting & Exhibit, Reno, Nevada, January 14-17, 2002.
11. Bogstad, M.C., Habashi, W.G., Akel, I., Ait-Ali-Yahia, D., Giannias, N., and Longo, V., "Computational-Fluid-Dynamics Based Advanced Ship-Airwake Database for Helicopter Flight Simulators," *Journal of Aircraft*, Vol.39, No.5, September-October 2002.
12. Camelli, F.E., Soto, O., Lohner, R., Sandberg, W.C., and Ramamurti, R., "Topside LPD17 Flow and Temperature Study with an Implicit Monolithic Scheme," AIAA Paper 2003-0969, 41st AIAA Aerospace Sciences Meeting & Exhibit, Reno, Nevada, January 6-9, 2003.
13. Wilkinson, C. and Roscoe, M.F., "DIMSS - JSHIP's Modeling and Simulation Process for Ship/Helicopter Testing and Training," AIAA Paper 2002-4597, AIAA Modeling and Simulation Technologies Conference and Exhibit, Monterey, CA, Aug. 5-8, 2002.
14. Wilkinson, C.H., Roscoe, M.F. and VanderVliet, G.M., "Determining Fidelity Standards for the Shipboard Launch and Recovery Task," AIAA Paper 2001-4062, AIAA Modeling and Simulation Technologies Conference and Exhibit, Montreal, Canada, Aug. 6-9, 2001.
15. He, C., Kang, H., Carico, D. and Long, K., "Development of a Modeling and Simulation Tool for Rotorcraft/Ship Dynamic Interface Testing,"

- American Helicopter Society 59th Annual Forum, Montreal, Canada, June 11-13, 2002.
16. Xin, H. and He, C., "A Combined Technique for Inverse Simulation Applied to Rotorcraft Shipboard Operations," American Helicopter Society 58th Annual Forum, Montreal, Canada, June 11-13 2002.
 17. Kleinman, D.L., Baron, S. and Levison, W.H., "An Optimal control Model of Human Response Part I: Theory and Validation", *Automatica*, Vol.6, No. 3, 1970.
 18. Hess, R.A., "Feedback control Models – Manual Control and Tracking," *Handbook of Human Factors and Ergonomics*, 2nd ed. Ed: G. Salvendy, Wiley, New York, 1997.
 19. Bradley, R. and Turner, G., "Simulation of the Human Pilot applied at the Helicopter/Ship Dynamic Interface," American Helicopter Society 55th Annual Forum, Montreal, Canada, May 1999.
 20. Lee, D. and Horn, J.F., "Simulation and Control of Helicopter Shipboard Launch and Recovery Operations", American Helicopter Society Flight Controls and Crew System Design Specialists' Meeting, Philadelphia, PA, USA, October 9-11, 2002.
 21. Lee, D., Sezer-Uzol, N., Horn, J.F., and Long, L.N., "Simulation of Helicopter Shipboard Launch and Recovery Operations Using Time-Accurate Airwakes", American Helicopter Society 59th Annual Forum, Phoenix, AZ, May 2003.
 22. Modi, A., Sezer-Uzol, N., Long, L.N., and Plassmann, P.E., "Scalable Computational Steering System for Visualization of Large-Scale CFD Simulations," AIAA Paper 2002-2750, 32nd AIAA Fluid Dynamics Conference and Exhibit, St. Louis, Missouri, 24–27 June 2002.
 23. Souliez, F.J., "Parallel Methods for the Computation of Unsteady Separated Flows Around Complex Geometries," *PhD Thesis, Dept. of Aerospace Engineering, The Pennsylvania State University*, August 2002.
 24. Howlett, J.J., "UH-60A BLACK HAWK Engineering Simulation Program: Volume I – Mathematical Model", NASA CR-177542, USAAVSCOM TR 89-A-001, September 1989.
 25. He, C, "Development and Application of a Generalized Dynamic Wake Theory of Lifting Rotors," Ph.D. Thesis, School of Aerospace Engineering, Georgia Institute of Technology, Jul 1989.

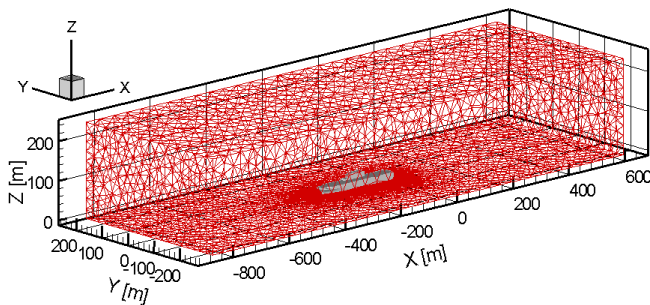


Figure 4 Unstructured grid domain around the LHA.

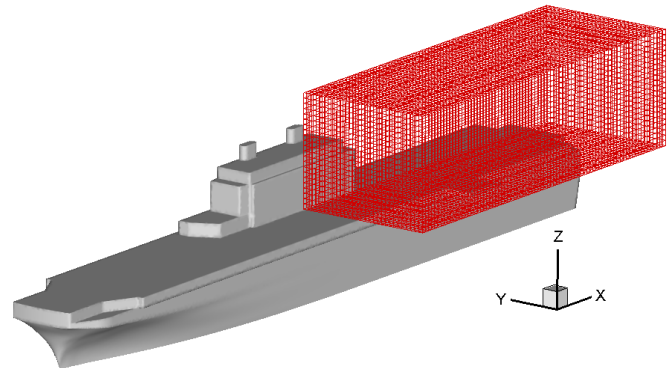
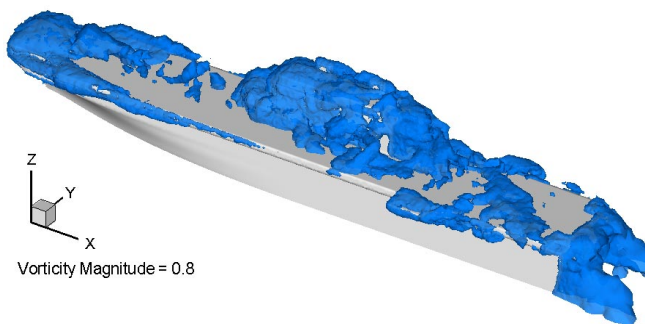
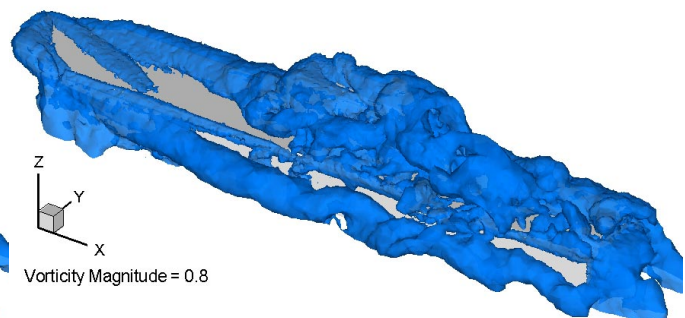


Figure 5 Rectangular volumetric domain of CFD data at the rear deck of LHA for DI simulations.



(a)



(b)

Figure 6 Vorticity magnitude iso-surface at $t = 40$ seconds
a) 0 degree WOD case b) 30 degrees WOD case

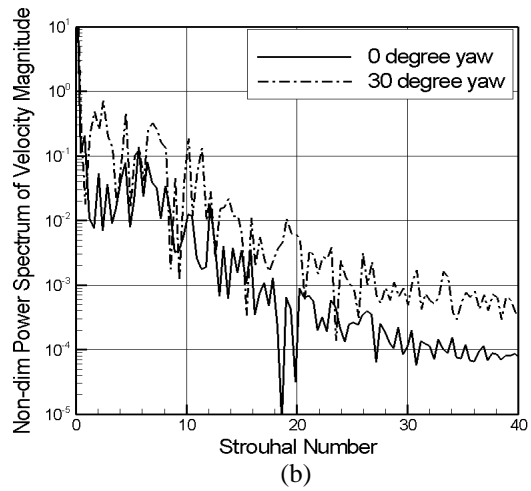
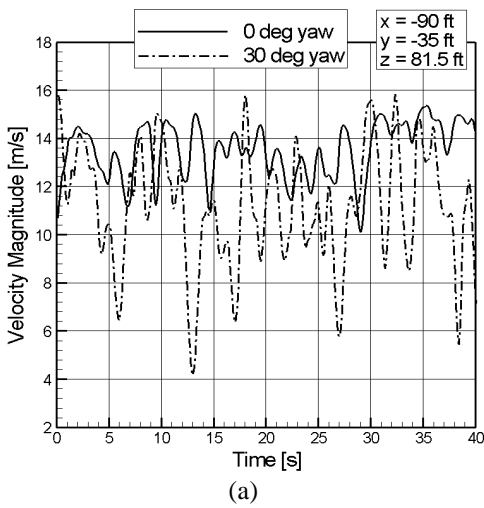


Figure 7 (a) Time history and (b) Non-dimensional Power spectrum of velocity magnitude at a selected point in the DI mesh from the CFD data over landing spot 8 for 0 and 30 degrees yaw cases.

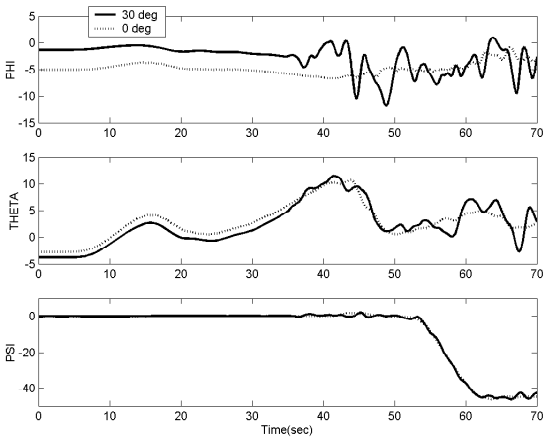


Figure 8 Helicopter attitude response (deg) for approach operations - Case 1 Pilot Model

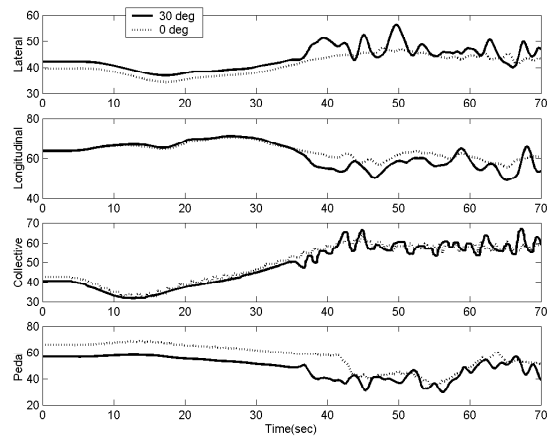


Figure 10 Control input responses (%) for approach operation - Case 1 Pilot Model

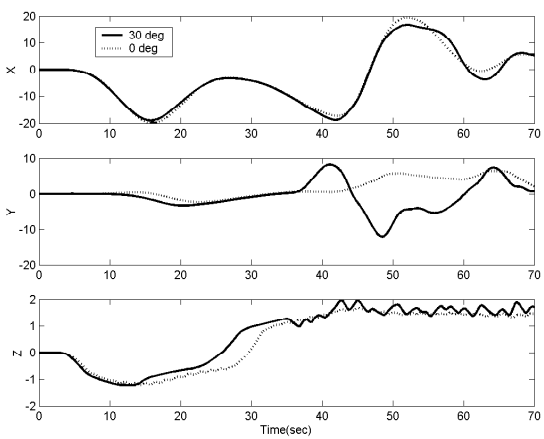


Figure 9 Position errors (ft) for approach operation - Case 1 Pilot Model

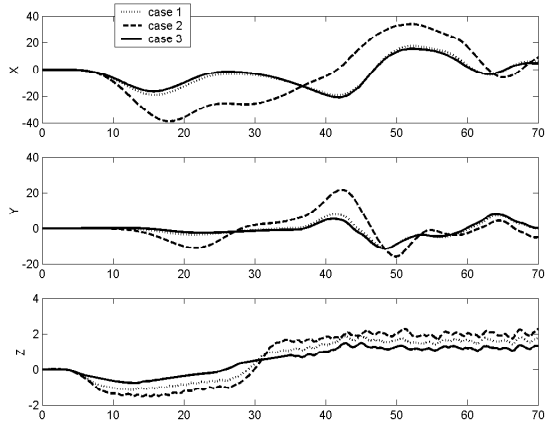


Figure 11 Position errors (ft) for approach operation - 30 deg WOD

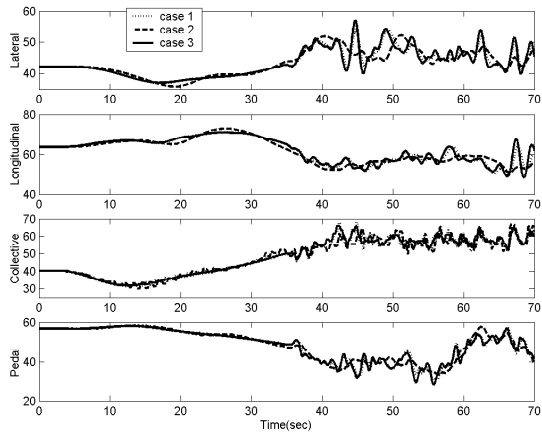


Figure 12 Control input responses (%) for approach operation - 30 deg WOD

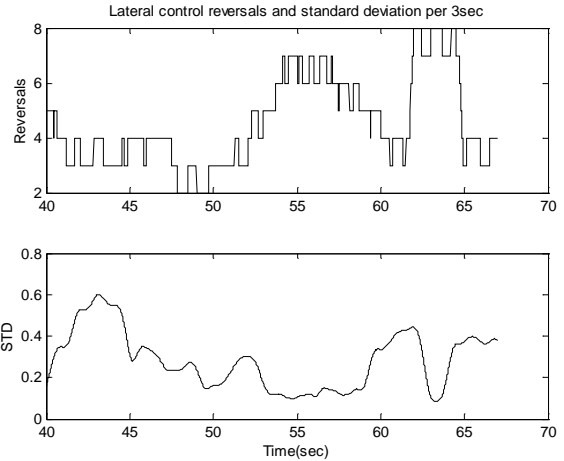


Figure 15 Lateral axis workload metrics for approach 30° WOD, Case 3 Pilot Model

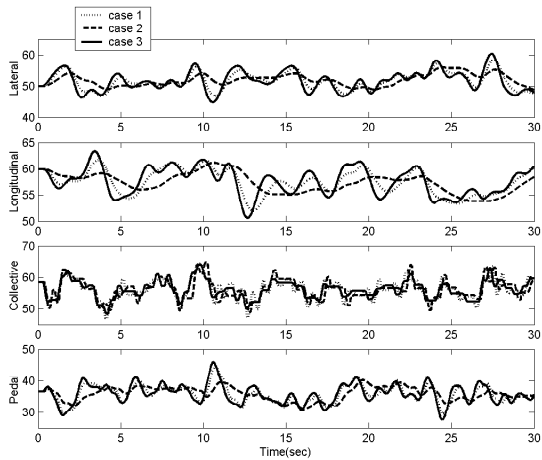


Figure 13 Control input responses (%) for hovering over landing spot 8 - 30 deg WOD

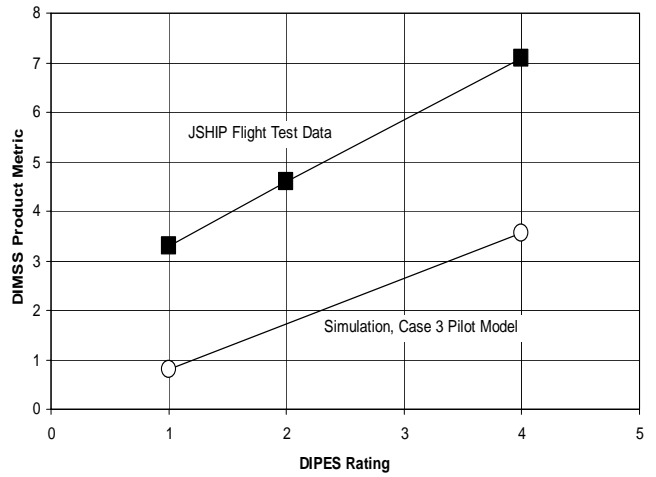


Figure 16 DIMSS Product Metric for Lateral Axis

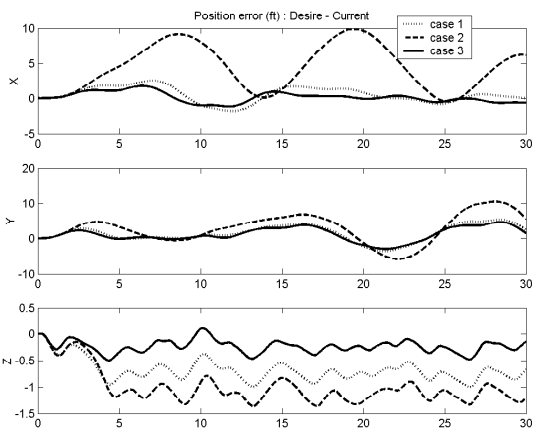


Figure 14 Position errors (ft) for hovering over landing spot 8 - 30 deg WOD

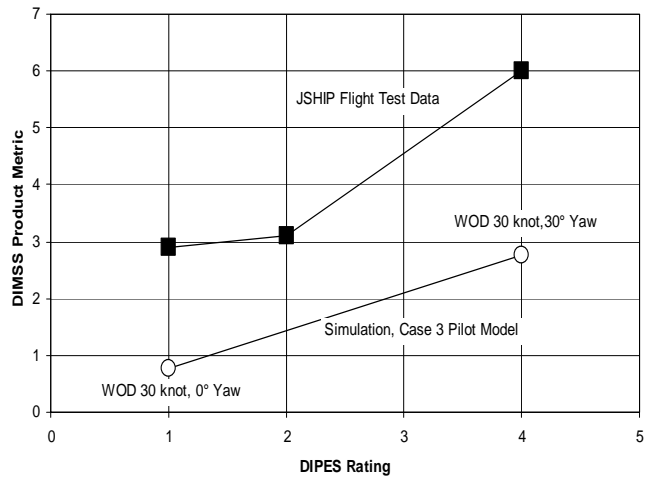


Figure 17 DIMSS Product Metric for Long. Axis